ACS APPLIED MATERIALS & INTERFACES

Research Article

www.acsami.org

Inorganic–Organic Shape Memory Polymer (SMP) Foams with Highly Tunable Properties

Dawei Zhang,[†] Keri M. Petersen,[‡] and Melissa A. Grunlan*[,†,‡]

[†]Materials Science and Engineering Program and [‡]Department of Biomedical Engineering, Texas A&M University, College Station, Texas 77843, United States

Supporting Information

ABSTRACT: Thermoresponsive shape memory polymers (SMPs) are a class of smart materials that can return from a temporary to a permanent shape with the application of heat. Porous SMP foams exhibit unique properties versus solid, nonporous SMPs, enabling their utility in different applications, including some in the biomedical field. Reports on SMP foams have focused on those based on organic polymer systems. In this study, we have prepared inorganic–organic SMP foams comprising inorganic polydimethylsiloxane (PDMS) segments and organic poly(ε-caprolactone) PCL segments. The PCL segments served as switching segments to induce shape changing behavior whereas the length of the PDMS soft segment was systematically tuned. SMP foams were formed via the photochemical cure of acrylated (AcO) macromers AcO-PCL$_{40}$-*block*-PDMS$_m$-*block*-PCL$_{40}$-OAc (m = 0, 20, 37, 66 and 130) using a revised solvent casting/particulate leaching (SCPL) method. By varying the PDMS segment length, PDMS-PCL foams having excellent shape memory behavior were obtained that exhibited highly tunable properties, including pore size, % porosity, compressive modulus, and degradation rate.

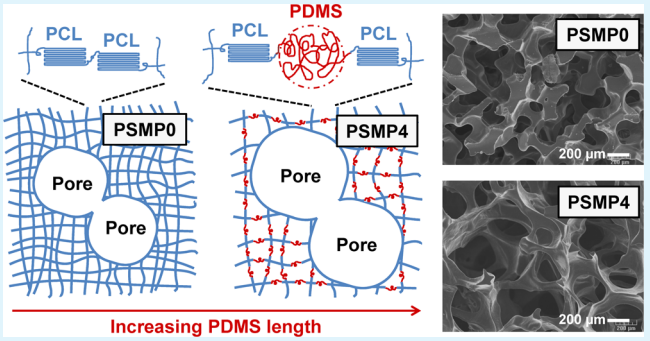

KEYWORDS: *shape memory polymers, foams, porous materials, poly(ε-caprolactone), polydimethylsiloxane*

INTRODUCTION

Thermoresponsive shape memory polymers (SMPs) are stimuli-sensitive materials whose shape is modulated by heat.[1,2] This entropically driven process is governed by the cooperative actions of the netpoints and switching segments. The netpoints, physical or chemical cross-links, establish the permanent shape whereas the "switching segments" actuate shape change when cycled through their thermal transition temperature (T_{trans}). T_{trans} may either be a glass transition temperature (T_g) or a melting transition temperature (T_m). Thus, a temporary shape formed by deforming at $T > T_{trans}$ can be fixed by cooling to $T < T_{trans}$ and then recovered by heating again to $T > T_{trans}$.

Solid, nonporous SMPs have been explored for various "self-deploying" biomedical devices, including those which may be implanted via minimally invasive surgeries,[3] such as smart sutures,[3] vascular stents,[4−7] bladder sensors,[8] and orthopedic anchors.[6,9,10] Porous SMP foams are desirable for applications requiring diffusivity and permeability, such as embolic sponges to treat aneurysms[11] and tissue engineering scaffolds.[12] In addition, compared to solid SMPs, SMP foams are lightweight and highly compressible and exhibit enhanced thermal actuating properties due to their permeability to heat.[11,13−18]

The utility of SMP foams is governed not only by their shape memory behavior, but also by their mechanical properties (e.g., modulus) and pore features (e.g., % porosity and interconnectivity). These properties are determined by both the chemical nature of the SMP and the method by which SMP foams are fabricated. Like solid SMPs, SMP foams have been limited to those based on organic polymers, including polyurethanes (PU)[11,13,14,19−21] and epoxies.[17,22] Thermoplastic PU SMP foams exhibit tunable T_{trans} values ($T_{trans} = T_g$: from −70 to 70 °C)[23] based on polymer structure and have been explored for aneurysm occlusion.[14,24,25] Thermosetting epoxy SMP foams have also been prepared,[17,22,26] but their high T_{trans} ($T_{trans} = T_g \approx 90$ °C) and brittle mechanical properties limit their use. Reports on utilizing fabrication strategies to further tailor the SMP foam properties are limited. For PU foams, different foaming techniques including coextrusion with chemical blowing agents, salt coextrusion/particulate leaching and solvent casting/particulate leaching (SCPL) have been reported to alter pore morphology and thermomechanical properties.[12] Highly cross-linked, ultralow density PU foams with interconnected pore morphologies were produced via gas foaming.[21] Recently, SMP foams have also been produced by emulsion templating of long side-chain polyacrylates and polymethacrylates and exhibited good shape recovery behavior.[27]

Received: October 22, 2012
Accepted: December 10, 2012
Published: December 10, 2012

SMP foams based on poly(ε-caprolactone) (PCL) are of particular interest in biomedical applications due to PCL's biocompatibility, biodegradability and elasticity.[28,29] The T_m of PCL serves as the T_{trans} which is conveniently tuned from 43 to 60 °C as the number average molecular weight (M_n) is increased.[30] For solid PCL-based SMPs, composites have been explored to achieve a broader range of properties.[31−34] Alternatively, AB polymer networks containing two distinct polymer segments have been prepared though incorporation of organic hard segments[3,35−37] or soft[38,39] segments whose T_g's are respectively higher and lower than that of PCL (T_g = −60 °C). In contrast, we have reported solid inorganic−organic SMPs comprised of inorganic polydimethylsiloxane (PDMS) soft segments (T_g = −125 °C[40]) and organic PCL switching segments.[41,42] These SMPs were formed by photochemical cure of a series of solvent casted acrylated (AcO) triblock macromers (AcO-PCL$_n$-*block*-PDMS$_m$-*block*-PCL$_n$-OAc). Varying the PCL[41] and PDMS[42] segment lengths resulted in tunability of mechanical properties of the resulting SMPs without compromising shape memory behavior (T_{trans}: from 50 to 53 °C).

Porous PCL SMP foams have been prepared via supercritical carbon dioxide foaming.[43] Porous PCL-based materials, generally targeted for tissue engineering scaffolds, have been produced by a variety of methods such as SCPL,[44] phase separation,[45,46] emulsion templating,[47] electrospinning,[48] and rapid prototyping.[49] More recently, we prepared porous inorganic−organic SMP foams from a single macromer composition (AcO-PCL$_{40}$-*block*-PDMS$_{37}$-*block*-PCL$_{40}$-OAc) using a revised SCPL method which included photo-cross-linking and salt fusion.[50] By tuning the fabrication variables such as salt size, degree of salt fusion and macromer concentration in solvent, we demonstrated that this macromer can be engineered into a series of SMP foams having excellent shape fixity (R_f) and highly tunable pore size, pore interconnectivity, modulus and percent shape recovery (R_r).

In this study, inorganic−organic SMP foams were prepared from a series AcO-PCL$_{40}$-*block*-PDMS$_m$-*block*-PCL$_{40}$-OAc macromers of variable PDMS segment lengths (m = 0, 20, 37, 66 and 130) using the aforementioned revised SCPL method. While maintaining the salt size and salt fusion parameters, PDMS-PCL SMP foams were produced with highly interconnected pores but varying size due to different extents of foam shrinkage during fabrication. In addition, the compressive modulus of the SMP foams was broadly tuned resulting in relatively soft to rigid foams. Shape fixity of the foams was excellent as was shape recovery, particularly after the first shape memory cycle. Finally, the degradation rates of the foams under accelerated conditions were highly dependent on macromer composition and corresponding pore size and cross-link density.

EXPERIMENTAL SECTION

Materials. Poly(dimethylsiloxane)-bis(3-aminopropyl) terminated (NH$_2$−PDMS$_m$−NH$_2$; m = 20 M_n = 1728 g/mol and m = 66, M_n = 5132 g/mol) were obtained from Gelest. NH$_2$−PDMS$_{130}$−NH$_2$ (M_n = 9868 g/mol) was synthesized as previously reported.[42] NH$_2$−PDMS$_{37}$−NH$_2$ (M_n = 2986 g/mol), polycaprolactone diol (PCL-diol; M_n ≈ 10 000 g/mol), ε-caprolactone, triethylamine (Et$_3$N), acryloyl chloride, 4-dimethylaminopyridine (DMAP), stannous 2-ethylhexanoate, 2,2-dimethoxy-2-phenylacetophenone (DMP), 1-vinyl-2-pyrrolidinone (NVP), sodium chloride (NaCl), sodium hydroxide (NaOH), and solvents were obtained from Sigma-Aldrich. Anhydrous magnesium sulfate (MgSO$_4$) was obtained from Fisher. Reagent-grade CH$_2$Cl$_2$ (dichloromethane, DCM) and NMR grade CDCl$_3$ were dried over 4 Å molecular sieves before use. All M_n values were determined by ^{1}H NMR end-group analysis.

Macromer Synthesis. Photo-cross-linkable macromers AcO-PCL$_{40}$-*block*-PDMS$_m$-*block*-PCL$_{40}$-OAc with constant number of repeat units (n = 40) for PCL segment length but varied PDMS segment length (**smp1:** m = 20; **smp2**: m = 37; **smp3**: m = 66; **smp4**: m = 130) were synthesized as previously reported.[41,42] Briefly, HO-PCL$_{40}$-*block*-PDMS$_m$-*block*-PCL$_{40}$−OH was prepared via ring-opening polymerization of ε-caprolactone in the presence of NH$_2$−PDMS$_m$−NH$_2$ and stannous 2-ethylhexanoate. The hydroxyl end-groups were subsequently acrylated by reacting with acryloyl chloride. PCL-diol (M_n ≈ 10 000 g/mol) was likewise acrylated to yield photo-cross-linkable PCL-diacrylate (**smp0**: m = 0; n = 44). ^{1}H NMR spectra were in agreement with those previously reported.[41,42]

Fabrication of SMP Foams. Porous SMP foams having variable PDMS segment lengths (**PSMP0:** m = 0; **PSMP1**: m = 20; **PSMP2**: m = 37; **PSMP3**: m = 66; **PSMP4**: m = 130) were fabricated via the previously described revised SCPL method.[50] NaCl particles were sieved with openings of 425 μm to collect 459 ± 69 μm sized particles. The average size was determined from SEM images with ImageJ software (http://rsb.info.nih.gov/ij/).

To prepare one cylindrical foam, 1.8 g of NaCl salt particles were placed inside a 3 mL glass vial (I.D. = 12.9 mm). Salt fusion was achieved by treating with water. First, 7.5 wt % DI water was added to the salt and the mixture was mechanically stirred. Second, the sealed vial was centrifuged (4000 rpm for 15 min) and air-dried overnight. A macromer solution (0.15 g/mL in DCM) was prepared and combined with 15 vol% photoinitiator solution (10 wt % DMP in NVP). The solution (0.6 mL) was then added to cover the salt and the vial centrifuged (2500 rpm for 10 min) to aide diffusion. The vial was then exposed to UV light (6 mW/cm^2, 365 nm) for 3 min. After air-drying overnight, the SMP foam cylinder was removed from the vial and the salt was leached out by soaking in water/ethanol mixture (1:1 vol:vol) for 4 days with daily changes of solvent and subsequently air-dried overnight. Lastly, the foam was heat treated at 85 °C for 1 h and cooled to room temperature (RT).

Differential Scanning Calorimetry (DSC). The % crystallinity of PCL segments in the SMP foams was determined by DSC (TA Instruments Q100). SMP foams specimens (5−10 mg) were sealed in hermetic pans which were then heated from −30 to 90 °C at 5 °C/min under a N$_2$ environment. T_m (i.e., T_{trans}) and enthalpy change (ΔH_m) of PCL (i.e., switching segments) was determined from the endothermic melting peak. The % crystallinity was calculated using the equation

$$\%\text{crystallinity} = \frac{\Delta H_m}{\Delta H_m^0} \times 100$$

where ΔH_m is normalized based on the % mass of PCL segments in the PDMS-PCL macromer. ΔH_m^0 is 139.5 J/g for 100% crystalline PCL.[51] The reported results are an average of three measurements.

Porosity. The % porosity (%P) of SMP foams was determined using the following equation:

$$P(\%) = \frac{\rho_{\text{solid SMP}} - \rho_{\text{porous SMP}}}{\rho_{\text{solid SMP}}} \times 100$$

For **smp0−4**, the density (ρ) of the corresponding solid, nonporous SMPs ($\rho_{\text{solid SMP}}$) were gravimetrically determined to be 1.119, 1.117, 1.114, 1.087, and 1.063 g/cm^3, respectively. The reported %P results are an average of three measurements.

Pore Morphology. Scanning electronic microscopy (SEM) was used to evaluate SMP foam pore size and pore interconnectivity. Foams were first freeze-fractured in liquid N$_2$ and cross sections then subjected to Au−Pt coating (~4 nm). SEM images were obtained with a JEOL 6400 SEM at an accelerating voltage of 15 kV. The average pore size was determined from SEM images (Figure 2, five pores measured per image) with ImageJ software.

Compressive Modulus. The compressive modulus (E) of cylindrical foams were measured at RT ($<T_{trans}$) with an Instron

Table 1. Compositions, % Diameter Change after Heat Treatment, and Thermal Properties of SMP Foams

sample	PCL (n)	PDMS (m)	M_n[a] (g/mol)	% mass of PCL segments	diameter change after heat treatment (%)	% crystallinity of PCL segments	T_m (°C)
PSMP0	44	0	10 138	100	24	61.5 ± 0.6	56.9 ± 0.0
PSMP1	40	20	10 956	84.3	29	59.9 ± 0.8	53.4 ± 0.0
PSMP2	40	37	12 214	75.6	24	59.9 ± 1.1	52.4 ± 0.2
PSMP3	40	66	14 360	64.3	15	56.4 ± 0.7	52.2 ± 0.1
PSMP4	40	130	19 096	48.3	11	65.3 ± 1.2	52.2 ± 0.0

[a]Per refs 41 and 42.

3345. Specimens were subjected to a constant strain rate of 1.5 mm/min up to 85% strain. In addition, E was also measured at 60 °C ($>T_{trans}$) with a dynamic mechanical analyzer (DMA, TA Instruments Q800). In this case, the foam cylinder was equilibrated at 60 °C prior to application of a constant strain (50%/min). For both analyses, E values were determined from the initial linear portion of the resulting stress−strain curves. The reported E values are an average of three measurements.

Shape Memory Properties. Shape memory properties were quantified via strain-controlled cyclic-thermal mechanical compression tests over two cycles (N) (TA Instrument Q800 DMA). The cylindrical foams were subjected to the following sequence: (1) after equilibrating at 60 °C (T_{high}) for 5 min, compress to a maximum strain (ε_m = 50%) at a rate of 50%/min, (2) hold at ε_m for 5 min and then cool to 25 °C (T_{low}) to fix the temporary shape, (3) remove the load and immediately measuring ε_u and (4) reheat to 60 °C (T_{high}) to recover the permanent shape, measure the recovered strain (ε_p). To start the second cycle, the specimen was subsequently cooled to RT, reheated to 60 °C and then compressed to 50% of the height recovered during the first cycle. The shape fixity (R_f) and shape recovery (R_r) for the first (N = 1) and second (N = 2) cycles were calculated using the following equations:

$$R_f(N) = \frac{\varepsilon_u(N)}{\varepsilon_m}$$

$$R_r(N) = \frac{\varepsilon_m - \varepsilon_p(N)}{\varepsilon_m - \varepsilon_p(N-1)}$$

where $\varepsilon_u(N)$ is the ultimate strain in the stress-free state in the fixing process. ε_m is the maximum compressive strain (50%). $\varepsilon_p(N-1)$ and $\varepsilon_p(N)$ are the final strains of the specimen in the two successive cycles in the stress-free state during the shape recovery process. For N = 1, $\varepsilon_p(0)$ equals "zero". The reported R_f and R_r for values are an average of three measurements.

Accelerated Degradation Tests. Each cylindrical foam was immersed in 20 mL of 1 M NaOH in a sealed centrifuge tube and maintained at 37 °C in a temperature controlled water bath. Every 12 h (up to 60 h), the specimens were removed (or liquid decanted if the specimen broke into pieces), thoroughly rinsed with DI water, blotted with a Kim Wipe and dried in vacuo (30 in. Hg, RT, ~7 h). After recording weight of the dried specimen (or specimen pieces), it was returned to freshly replenished 1 M NaOH.

RESULTS AND DISCUSSIONS

Fabrication. To fabricate **PSMP0−4** foams, we selected the following SCPL parameters: salt size (459 ± 69 μm), salt fusion (7.5 wt % water added to salt) and macromer concentration in DCM (0.15 g/mL) (Table 1). These parameters were chosen as they were previously determined to be effective to produce highly interconnected pores for SMP foams based on AcO-PCL$_{40}$-*block*-PDMS$_{37}$-*block*-PCL$_{40}$-OAc.[50] While all SMP foams were fabricated in vials of a constant I.D. (12.9 mm), foam diameters varied with PDMS segment length as well as before and after heat treatment. Prior to heat treatment, foam diameters increased with higher PDMS segment length (see Figure S1 in the Supporting Information). Heat treatment, the final step of foam fabrication, caused additional foam shrinkage but was previously determined to be essential for shape memory behavior for these SMP foams.[50] This is attributed to reorganization of PCL domains in closer proximity since, as confirmed in the former study,[50] PCL segment %crystallinity actually decreased following heat treatment. After heat treatment, the final diameter of SMP foams likewise increased with a higher PDMS segment length (Figure 1). For a given

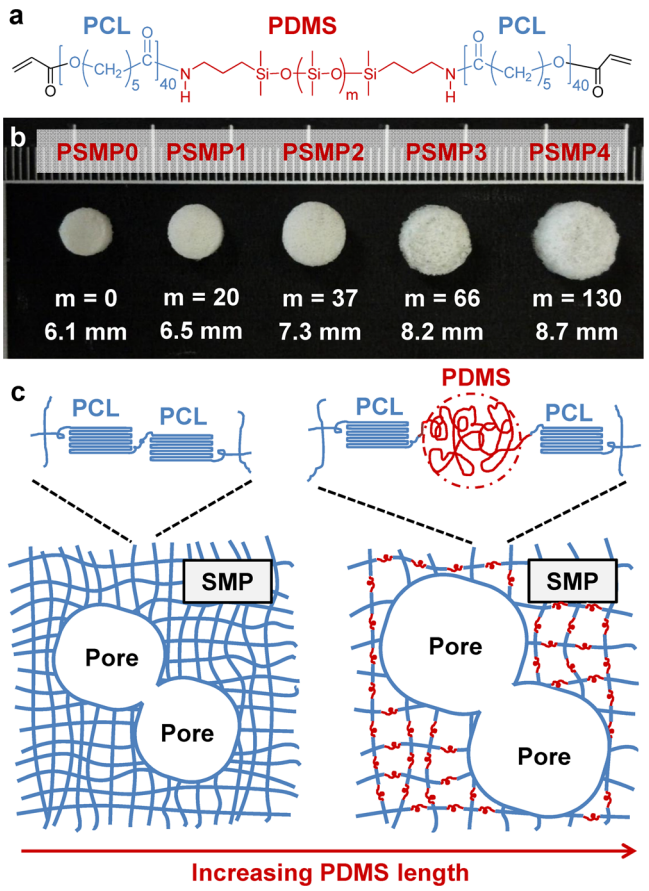

Figure 1. (a) Structure of PDMS-PCL macromers; (b) diameters of **PSMP0−4** (after heat treatment); (c) schematic depiction of the relationship between PDMS segment length, network cross-link density and pore size.

SMP foam composition, the % change in diameter following heat treatment also generally decreased with increased PDMS segment length (Table 1). As depicted in Figure 1c, the differences in foam diameter may be attributed to the greater separation of PCL crystalline domains by longer PDMS soft segments.

dx.doi.org/10.1021/am302426e | ACS Appl. Mater. Interfaces 2013, 5, 186−191

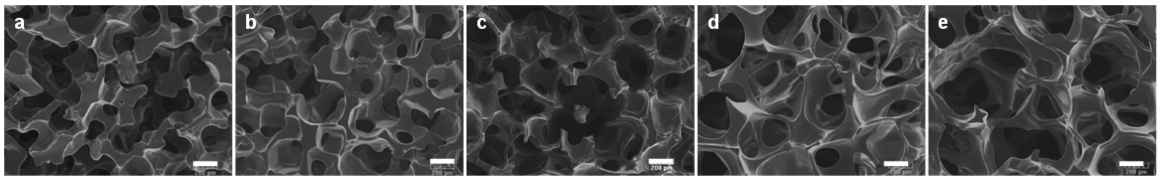

Figure 2. SEM images of (a–e) **PSMP0–4**. Scale bars = 200 μm.

Pore Size and Interconnectivity. While **PSMP0–4** were fabricated with the same salt size, their pore sizes varied substantially (Figure 2). For **PSMP0–4**, average pore sizes are estimated to be ~200, ~250, ~300, ~400, and ~450 μm, respectively. The systematic increase in pore size from **PSMP0** (m = 0) to **PSMP4** (m = 130) corresponds to the associated decrease in shrinking (i.e., greater foam specimen diameter) with increased PDMS segment length. Because of high level of salt fusion (i.e., 7.5 wt % water added to salt), all SMP foams exhibited a high degree of pore interconnectivity.

Thermal Properties. The % crystallinity and T_m (i.e., T_{trans}) of the PCL crystalline domains of **SMP0–4** were determined by DSC (Table 1). As the length of the PDMS segment increased, % crystallinity of PCL segments were similar in **PSMP0–4** due to their constant repeat unit length (n) of 40. PCL T_m slightly decreased from 56.9 °C (**PSMP0**) to 52.2 °C (**PSMP4**). Thus, as the length of the PDMS segments were increased, crystallization of PCL segments was largely undisrupted. However, the foams were less crystalline overall due to decrease in % mass of PCL from **PSMP0** to **PSMP4**.

Shape Memory Properties. Strain-controlled thermomechanical compression tests of **PSMP0–4** were used to determine shape recovery (R_r) and shape fixity (R_f) for two cycles (N = 1 and 2). For the first cycle, R_r dramatically decreased as the PDMS segment length was increased from **PSMP0** (m = 0) to **PSMP4** (m = 130) (Figure 3). For a given SMP foam, R_r increased from cycle 1 to cycle 2 and was greater as the PDMS segment length increased (Figure 3). An increase in R_r after the first shape memory cycle has been previously reported for nonporous[33,38] as well as porous[43,50] SMPs. The decrease in R_r with increased PDMS segment length corresponds with a decrease in % mass of PCL and, hence, the amount of PCL crystalline domains (i.e., the switching segments) in the PDMS-PCL foams. In addition, this is accompanied by decreased shrinkage of the foams (i.e., a larger foam diameter, per Figure 1). Thus, as expected, greater %mass of PCL in the foams and enhanced proximity of PCL switching segments improve R_r. However, even **PSMP4** exhibits a reasonably high R_r during cycle 2. Thus, to maximize shape recovery during, for instance, implantation, SMP foams should first be "pre-conditioned" by conducting one shape memory cycle. The shape recovery process for **PSMP3** is shown in Figure 4. The **PSMP3** cylindrical foam (~15 mm diameter × ~9 mm height) was heated at 60 °C, compressed into a temporary shape (~1 mm in thickness) and cooled to *RT*. After affixing to a needle, the compressed foam was submerged into a warm water bath where it expanded to its permanent shape in ~10 s.

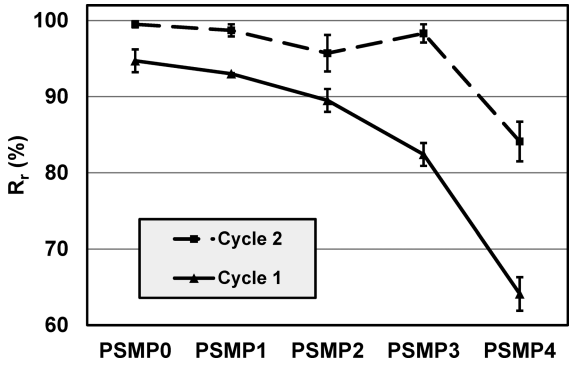

Figure 3. Shape recovery (R_r) of **PSMP0–4** for two cycles (N = 1 and 2). Standard deviations are calculated based on three measurements (n = 3) for each composition.

For cycles 1 and 2, R_f was just slightly >100% for all SMP foams (see Table S1 in the Supporting Information). In our previous study as well as in another report, R_f values >100% were reported for PCL-based SMP foams.[43,50] This may be attributed to a slight increase in compressive strain during shape fixation that occurs as a result of recrystallization of PCL segments into more compact structures[43] or to compression-induced recrystallization of PCL.

Compressive Modulus and % Porosity. SMPs with broadly tunable moduli yet with T_{trans} values tolerated by biological tissues are desirable to meet the requirements of a range of biomedical applications. However, for PU SMP foams for instance,[17,22,26] the modulus is typically increased by increasing the T_g (i.e., T_{trans}) of the switching segments. In contrast, the reported inorganic–organic SMP foams exhibit a broad range of compressive modulus (E) values while maintaining very similar T_{trans} values (~53 °C) (Table 1). E was measured at 60 °C (>T_{trans}) (Figure 5) and at *RT* (<T_{trans}) (Figure 6) to assess the relatively stiffness during shape recovery and in the permanent rigidized state, respectively. At both temperatures, as the PDMS segment length was increased,

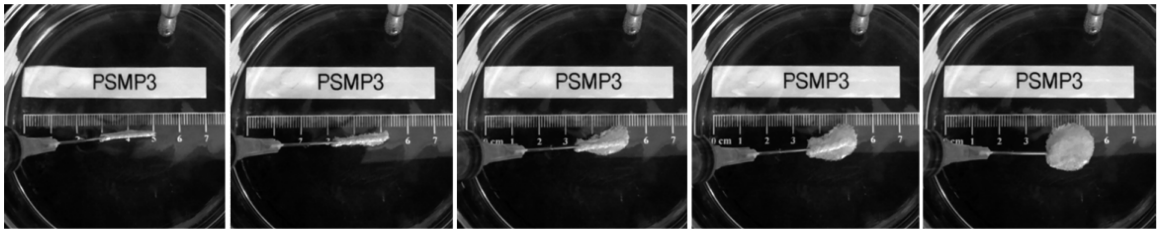

Figure 4. Photo series showing the shape recovery of **PSMP3** when submerged in a ~55 °C water bath. The time interval between panes is ~2 s.

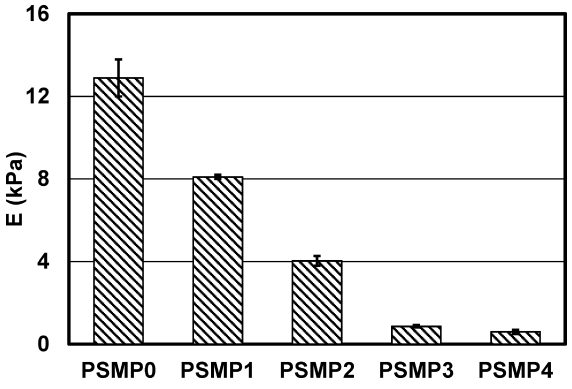

Figure 5. Compressive modulus (E) values of **PSMP0−4** at 60 °C. Standard deviations are calculated based on three measurements (n = 3) for each composition.

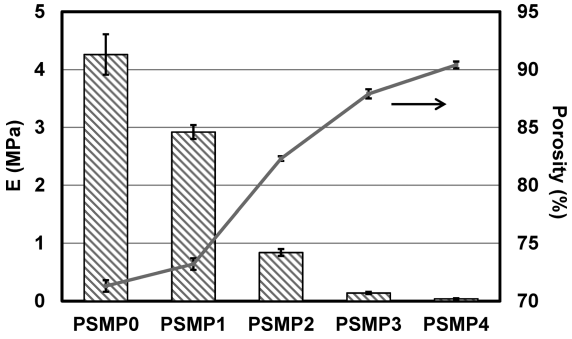

Figure 6. Compressive modulus (E) and % porosity values of **PSMP0−4** at RT. Standard deviations are calculated based on three measurements (n = 3) for each composition.

E was observed to systematically decrease. At 60 °C, the PCL crystalline domains have gone through their melt transition which gave rise to foams with low E values (from 0.6 to 12.9 kPa) (Figure 5). At RT, a range of E values from relative rigid (∼4.3 MPa; **PSMP0**) to soft (∼0.04 MPa; **PSMP4**) was observed. This trend can be attributed to not only an increase in the PDMS soft segment length, but also a corresponding decrease in the amount of PCL crystalline domains, a decrease in cross-link density (Figure 1) and increase in pore size (Figure 2). Related to these trends and also contributing to a decrease in E is the increase in % porosity ∼70% (**PSMP0**) to ∼90% (**PSMP4**) with increased PDMS segment length (Figure 6).

Accelerated Degradation Studies. PCL undergoes hydrolytic degradation via hydrolysis of ester bonds with complete resorption occurring slowly (>2 years).[52,53] Accelerated degradation tests conducted in a basic environment has been utilized to provide a more acceptable time frame.[53] As the PDMS segment length increased, the degradation (in terms of mass loss) occurred more rapidly (Figure 7) and differences were visually apparent (see Figure S2 in the Supporting Information). Notably, at 60 h, **PSMP3** and **PSMP4** cylindrical specimens had eroded into noncohesive fragments. This increase in degradation with PDMS segment length occurred despite the hydrophobicity of PDMS which typically reduces the rate of hydrolysis.[42] However, SMP foams prepared with longer PDMS segments contained reduced amounts of PCL crystalline domains and as well as a decrease in cross-link density and increased pore size, which facilitated water uptake and hence hydrolysis.

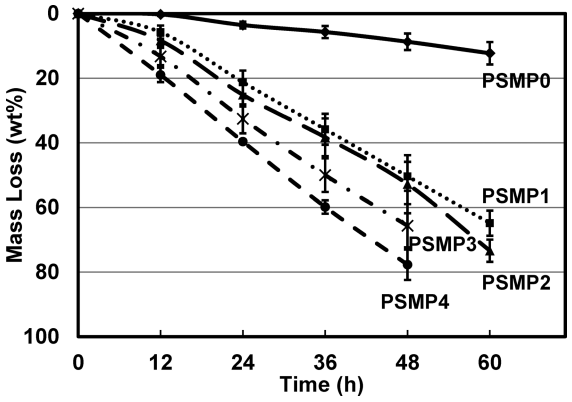

Figure 7. Mass loss of **PSMP0−4** in 1 M NaOH at 37 °C. Standard deviations are calculated based on three measurements (n = 3) for each composition.

CONCLUSIONS

To summarize, we prepared biodegradable inorganic−organic SMP foams (**PSMP0−4**) that comprised PCL switching segments and PDMS soft segments of variable lengths based on AcO-PCL$_{40}$-*block*-PDMS$_m$-*block*-PCL$_{40}$-OAc (m = 0, 20, 37, 66 and 130). SMP foams were produced via a revised SCPL process in which a given macromer was dissolved in DCM (0.15 g/mL) and cast over fused NaCl salt particles (459 ± 69 μm; fused with 7.5 wt % water) before photocuring. The PDMS soft segment length (m) had a significant impact on the chemical and physical properties of the SMP foams. Fabricated as cylinders, SMP foams exhibited less shrinkage as the PDMS segment length increased thereby producing a concomitant increase in % porosity and pore size. The shape fixity (R_f) of all foams were excellent (∼100%). Shape recovery (R_r) decreased with increasing PDMS segment length but, after the first cycle, all foams displayed R_r values > ∼85%. As expected given the low T_g of PDMS, the compressive modulus (E) decreased with PDMS segment length which was accompanied by a decrease in the amounts of PCL crystalline domains providing a series of foams that ranged from relatively soft to rather rigid. Finally, the degradation rate of the SMP foams increased with PDMS segment length due to the corresponding increase in pore size and decrease in cross-link density as well as the reduced amounts of PCL crystalline domains. Thus, these PDMS-PCL SMP foams provide those whose T_{trans} is maintained at ∼53 °C with excellent shape memory properties. However, a broad range of pore size, E values, and rate of degradation can be achieved by tuning the PDMS segment length. Such SMP foams are expected to be widely useful for exploring a variety of biomedical applications.

ASSOCIATED CONTENT

Supporting Information

Figure S1, photograph of **PSMP0−4** foams before heat treatment; Figure S2,photographs of **PSMP0−4** foams as a function of degradation time; and Table S1, shape fixities for **PSMP0−4** foams. This material is available free of charge via the Internet at http://pubs.acs.org.

AUTHOR INFORMATION

Corresponding Author

*E-mail: mgrunlan@tamu.edu.

Notes

The authors declare no competing financial interest.

REFERENCES

(1) Lendlein, A.; Kelch, S. *Angew. Chem., Int. Ed.* **2002**, *41*, 2034.
(2) Xie, T. *Polymer* **2011**, *52*, 4985.
(3) Lendlein, A.; Langer, R. *Science* **2002**, *296*, 1673.
(4) Wache, H. M.; Tartakowska, D. J.; Hentrich, A.; Wagner, M. H. *J. Mater. Sci. - Mater. Med.* **2003**, *14*, 109.
(5) Small, W.; Buckley, P. R.; Wilson, T. S.; Benett, W. J.; Hartman, J.; Saloner, D.; Maitland, D. J. *IEEE Trans. Biomed. Eng.* **2007**, *54*, 1157.
(6) Yakacki, C. M.; Shandas, R.; Safranski, D.; Ortega, A. M.; Sassaman, K.; Gall, K. *Adv. Funct. Mater.* **2008**, *18*, 2428.
(7) Xue, L.; Dai, S.; Li, Z. *Biomaterials* **2010**, *31*, 8132.
(8) Pereira, I. M.; Axisa, F.; Oréfice, R. L.; Vanfleteren, J.; Neves, H. P. *J. Biomed. Mater. Res. B* **2011**, *96B*, 369.
(9) Gall, K.; Yakacki, C. M.; Liu, Y.; Shandas, R.; Willett, N.; Anseth, K. S. *J. Biomed. Mater. Res. A* **2005**, *73A*, 339.
(10) Ware, T.; Ellson, G.; Kwasnik, A.; Drewicz, S.; Gall, K.; Voit, W. *J. Reinf. Plast. Compos.* **2011**, *30*, 371.
(11) Ortega, J.; Maitland, D.; Wilson, T.; Tsai, W.; Savaş, Ö.; Saloner, D. *Ann. Biomed. Eng.* **2007**, *35*, 1870.
(12) De Nardo, L.; Bertoldi, S.; Tanzi, M. C.; Haugen, H. J.; Farè, S. *Smart Mater. Struct.* **2011**, *20*, 035004.
(13) Tobushi, H.; Okumura, K.; Endo, M.; Hayashi, S. *J. Intell. Mater. Syst. Struct.* **2001**, *12*, 283.
(14) Metcalfe, A.; Desfaits, A.-C.; Salazkin, I.; Yahia, L. H.; Sokolowski, W. M.; Raymond, J. *Biomaterials* **2003**, *24*, 491.
(15) Tobushi, H.; Matsui, R.; Hayashi, S.; Shimada, D. *Smart Mater. Struct.* **2004**, *13*, 881.
(16) Huang, W. M.; Lee, C. W.; Teo, H. P. *J. Intell. Mater. Syst. Struct.* **2006**, *17*, 753.
(17) Di Prima, M. A.; Lesniewski, M.; Gall, K.; McDowell, D. L.; Sanderson, T.; Campbell, D. *Smart Mater. Struct.* **2007**, *16*, 2330.
(18) Chung, S. E.; Park, C. H. *J. Appl. Polym. Sci.* **2010**, *117*, 2265.
(19) Sokolowski, W. M.; Hayashi, S. *SPIE Proceedings of 10th International Symposium on Smart Structures and Materials*; International Society for Optics and Photonics: Bellingham, WA, 2003; p 534
(20) Witold, S.; Annick, M.; Shunichi, H.; L'Hocine, Y.; Jean, R. *Biomed. Mater.* **2007**, *2*, S23.
(21) Singhal, P.; Rodriguez, J. N.; Small, W.; Eagleston, S.; Van de Water, J.; Maitland, D. J.; Wilson, T. S. *J. Polym. Sci., Part B: Polym. Phys.* **2012**, *50*, 724.
(22) Di Prima, M. A.; Gall, K.; McDowell, D. L.; Guldberg, R.; Lin, A.; Sanderson, T.; Campbell, D.; Arzberger, S. C. *Mech. Mater.* **2010**, *42*, 405.
(23) Sokolowski, W. M.; Chmielewski, A. B.; Hayashi, S.; Yamada, T. *Proc. SPIE—Int. Soc. Opt. Eng.* **1999**, *3669*, 179.
(24) Maitland, D. J.; Small, W., IV; Ortega, J. M.; Buckley, P. R.; Rodriguez, J.; Hartman, J.; Wilson, T. S. *J. Biomed. Opt.* **2007**, *12*, 030504.
(25) De Nardo, L.; Alberti, R.; Cigada, A.; Yahia, L. H.; Tanzi, M. C.; Farè, S. *Acta Biomater.* **2009**, *5*, 1508.
(26) Fabrizio, Q.; Loredana, S.; Anna, S. E. *Mater. Lett.* **2012**, *69*, 20.
(27) Gurevitch, I.; Silverstein, M. S. *Soft Matter* **2012**, *8*, 10378.
(28) Middleton, J. C.; Tipton, A. J. *Biomaterials* **2000**, *21*, 2335.
(29) Sun, H.; Mei, L.; Song, C.; Cui, X.; Wang, P. *Biomaterials* **2006**, *27*, 1735.
(30) Wang, S.; Lu, L.; Gruetzmacher, J. A.; Currier, B. L.; Yaszemski, M. J. *Biomaterials* **2006**, *27*, 832.
(31) Zheng, X.; Zhou, S.; Li, X.; Weng, J. *Biomaterials* **2006**, *27*, 4288.
(32) Xiao, Y.; Zhou, S.; Wang, L.; Gong, T. *ACS Appl. Mater. Interfaces* **2010**, *2*, 3506.
(33) Luo, X.; Mather, P. T. *Macromolecules* **2009**, *42*, 7251.
(34) Liu, T.; Li, J.; Pan, Y.; Zheng, Z.; Ding, X.; Peng, Y. *Soft Matter* **2011**, *7*, 1641.
(35) Min, C.; Cui, W.; Bei, J.; Wang, S. *Polym. Adv. Technol.* **2005**, *16*, 608.
(36) Rabani, G.; Luftmann, H.; Kraft, A. *Polymer* **2006**, *47*, 4251.
(37) Nagata, M.; Yamamoto, Y. *J. Polym. Sci., Part A: Polym. Chem.* **2009**, *47*, 2422.
(38) Lendlein, A.; Schmidt, A. M.; Langer, R. *Proc. Natl. Acad. Sci. U.S.A.* **2001**, *98*, 842.
(39) Bellin, I.; Kelch, S.; Langer, R.; Lendlein, A. *Proc. Natl. Acad. Sci. U.S.A.* **2006**, *103*, 18043.
(40) Semlyen, J. A.; Clarson, S. J. *Siloxane Polymers*; Prentice Hall: Upper Saddle River, NJ, 1993.
(41) Schoener, C. A.; Weyand, C. B.; Murthy, R.; Grunlan, M. A. *J. Mater. Chem.* **2010**, *20*, 1787.
(42) Zhang, D.; Giese, M. L.; Prukop, S. L.; Grunlan, M. A. *J. Polym. Sci., Part A: Polym. Chem.* **2011**, *49*, 754.
(43) Madbouly, S. A.; Kratz, K.; Klein, F.; Lüzow, K.; Lendlein, A. *Mater. Res. Soc. Symp. Proc.* **2009**, *1190*, No. 1190-NN04-04.
(44) Mikos, A. G.; Thorsen, A. J.; Czerwonka, L. A.; Bao, Y.; Langer, R.; Winslow, D. N.; Vacanti, J. P. *Polymer* **1994**, *35*, 1068.
(45) Guan, L.; Davies, J. E. *J. Biomed. Mater. Res. A* **2004**, *71A*, 480.
(46) Ma, H.; Hu, J.; Ma, P. X. *Adv. Funct. Mater.* **2010**, *20*, 2833.
(47) Busby, W.; Cameron, N. R.; Jahoda, C. A. B. *Biomacromolecules* **2001**, *2*, 154.
(48) Mo, X. M.; Xu, C. Y.; Kotaki, M.; Ramakrishna, S. *Biomaterials* **2004**, *25*, 1883.
(49) Hollister, S. J. *Nat. Mater.* **2005**, *4*, 518.
(50) Zhang, D.; Burkes, W. L.; Schoener, C. A.; Grunlan, M. A. *Polymer* **2012**, *53*, 2935.
(51) Pitt, C. G.; Chasalow, F. I.; Hibionada, Y. M.; Klimas, D. M.; Schindler, A. *J. Appl. Polym. Sci.* **1981**, *26*, 3779.
(52) Yang, S.; Leong, K.-F.; Du, Z.; Chua, C.-K. *Tissue Eng.* **2001**, *7*, 679.
(53) Christopher, X. F. L.; Monica, M. S.; Swee-Hin, T.; Dietmar, W. H. *Biomed. Mater.* **2008**, *3*, 034108.